Results in Physics 13 (2019) 102180

Contents lists available at ScienceDirect

Results in Physics

journal homepage: www.elsevier.com/locate/rinp

High-throughput first-principles calculations as a powerful guiding tool for materials engineering: Case study of the AB_2X_4 (A = Be, Mg, Ca, Sr, ba; B = Al, Ga, in; X = O, S) spinel compounds

Y. Wang[a], W.-B. Chen[b], F.-Y. Liu[a], D.-W. Yang[a], Y. Tian[a], C.-G. Ma[a,*], M.D. Dramićanin[a,c,d], M.G. Brik[a,e,f,*]

[a] College of Sciences, Chongqing University of Posts and Telecommunications, Chongqing 400065, People's Republic of China
[b] Engineering Research Center of New Energy Storage Devices and Applications, Chongqing University of Arts and Sciences, Chongqing 402160, People's Republic of China
[c] University of Belgrade, Faculty of Physics, Studentski trg 12–16, Belgrade 11000, Serbia
[d] University of Belgrade, Vinča Institute of Nuclear Sciences, P.O. Box 522, Belgrade 11001, Serbia
[e] Institute of Physics, University of Tartu, W. Ostwald Str. 1, Tartu 50411, Estonia
[f] Institute of Physics, Jan Długosz University, Armii Krajowej 13/15, PL-42200 Częstochowa, Poland

ARTICLE INFO

Keywords:
First-principles calculations
Spinel compounds
Structural, Electronic, Elastic properties
Materials engineering

ABSTRACT

Modern methods of theoretical and experimental materials engineering can be greatly facilitated by reliably established guiding trends that set directions for a smart search for new materials with enhanced performance. Those trends can be derived from a thorough analysis of large arrays of the experimental data, obtained both experimentally and theoretically. In the present paper, the structural, elastic, and electronic properties of 30 spinel compounds AB_2X_4 (A = Be, Mg, Ca, Sr, Ba; B = Al, Ga, In; X = O, S) were investigated using the CRYSTAL14 program. For the first time the lattice constants, bulk moduli, band gaps and density of states for these 30 spinels were systematically calculated and analyzed. Influence of the cation and anion variation on the above-mentioned properties was highlighted. Several relations between lattice constants, bulk modulus and ionic radii, electronegativities of constituting ions were found. Several linear equations are proposed, which provide a convenient way to predict the lattice constants and bulk moduli of isostructural spinels.

Introduction

Sustainable development of the modern technological society to large extent is determined nowadays by the materials science progress. Understanding of the materials performance and possibilities of tuning their properties is of paramount importance for numerous applications, including the optical ones such as lighting, lasing, optical sensing, displays manufacturing, solar cell production etc. [1–9]. Among numerous groups of various materials, cubic spinels are of special practical interest because of their excellent thermal [10], chemical, optical properties [11–13] etc. They are also important for the electrical engineering applications, since the Li-bearing spinels such as lithium manganese oxides $LiMn_2O_4$ are good materials for the lithium batteries [14].

The spinel structure has two types of the cationic positions: the tetrahedral and the octahedral ones [15]. Taking the spinel general chemical formula as AB_2X_4, the cations distribution through the available sites can be as follows: the divalent cations A occupy the tetrahedral sites, whereas the trivalent cations B locate at the octahedral sites. However, there always exists a possibility for the cation interchange. There are the so-called the "normal" $A(B_2)X_4$ and "inverse" $B(AB)X_4$ spinels, where the ions in the parenthesis occupy the octahedral sites. As can be seen, in the inverse spinels all A cations interchange their tetrahedral sites with the half of the B cations from the octahedral positions. Very often the intermediate situations can be met, which are characterized by only a fractional interchange between the A and B cations. Simultaneous presence of two kinds of the cationic sites offers an opportunity of doping spinel compounds with various transition metal and rare earth ions for lighting applications, e.g. $ZnGa_2O_4:Cr^{3+}$ [16], $ZnAl_2O_4:Cr^{3+}$ and $MgAl_2O_4:Cr^{3+}$ [17], $MgAl_2O_4:Co^{2+}$ [18], $MgAl_2O_4:Mn^{2+}$ [19], $ZnAl_2S_4:V^{3+}$ [20] and $ZnAl_2S_4:Co^{2+}$ [21], $MgGa_2O_4:Cr^{3+}$ [22], $CoFe_2O_4:Dy^{3+}$ [23], $MgAl_2O_4:Eu^{3+}$ [24],

* Corresponding authors at: College of Sciences, Chongqing University of Posts and Telecommunications, Chongqing 400065, People's Republic of China (C.-G. Ma); Institute of Physics, University of Tartu, W. Ostwald Str. 1, Tartu 50411, Estonia (M.G. Brik).
E-mail addresses: cgma.ustc@gmail.com (C.-G. Ma), mikhail.brik@ut.ee (M.G. Brik).

https://doi.org/10.1016/j.rinp.2019.102180
Received 14 February 2019; Received in revised form 3 March 2019; Accepted 4 March 2019
Available online 07 March 2019

$Zn_xMg_{1-x}Fe_2O_4:Nd^{3+}$ [25].

Several other diverse applications of the spinel compounds can be also noticed, e.g. in 2006 Hong et al. fabricated ultra-long $ZnAl_2O_4$ spinel nanotubes [26]. Spinels with the 3d transition metal ions are of particular interest, since these ions may exhibit different valence states, occupy both cation sites and show magnetic properties. For example, in 2016 Wu et al. studied the $Co^{II}Fe^{III}Co^{III}O_4$ spinel with Fe and Co making an inverse spinel structure and found a remarkable oxygen reduction reaction activity [27]. In 2018 Prasad et al. synthesized MFe_2O_4 ($M = Mg^{2+}$, Zn^{2+}, Mn^{2+}) spinels and reported their structural, elastic and electron magnetic resonance properties [28]. Radiation stability of $MgAl_2O_4$ spinel was studied intensively [29] and references therein. Various first-principles calculations of different physical properties of spinels can be found in the literature, e.g. for CdX_2O_4 (X = Al, Ga, In) [30], MgX_2O_4 (X = Al, Ga, In) [31], $MgIn_2S_4$ and $CdIn_2S_4$ [32], $ZnAl_2S_4$ and $ZnGa_2O_4$ [33], MRh_2O_4 (M = Zn, Cd) [34] etc.

While detailed investigations of physical properties of individual representatives of the spinel compounds remain to be an important scientific and technological task, comparative studies – both experimental and theoretical – of a large number of isostructural materials conducted in one research paper with a consistent use of the same research techniques can reveal interesting and important correlations between the chemical composition and physical properties. Such "structure–property" and "property–property" relations become very popular recently, and their importance for materials science is constantly and rapidly growing. The reason is that these relations can effectively guide and direct experimental scientists in their smart search for new materials.

In the present paper we report the results of the high-throughput first-principles hybrid density functional theory (DFT)-based calculations of the structural, electronic, elastic, thermodynamic properties of 30 cubic AB_2X_4 (A = Be, Mg, Ca, Sr, Ba; B = Al, Ga, In; X = O, S) spinels. Among those 30 compounds, 26 are reported here for the first time, to the best of our knowledge. The initial structural data were taken from Ref. [35], where an empirical linear relation between the lattice constants, ionic radii and electronegativities for 185 spinels was established.

After having performed rigorous calculations, we analyzed the variations of the lattice constant, band gap, bulk moduli, elastic tensor constants, Debye temperature with chemical composition, which were visualized with the help of various two- and three-dimensional diagrams. The directions of variations of all these properties were linked with the chemical composition and changes of both cations and anions in the studied compounds.

The obtained results and linear relations between the ionic radii and electronegativities of the constituting elements, on the one side, and the lattice constants and bulk moduli, on the on the other side, have a strong predictive power and can facilitate search for new spinel compounds.

Computational details

The first-principles calculations of the structural, elastic and electronic properties of 30 cubic AB_2X_4 (A = Be, Mg, Ca, Sr, Ba; B = Al, Ga, In; X = O, S) spinels were implemented by employing the periodic ab initio CRYSTAL14 code based on the "linear combination of atomic orbits" method with local Gaussian-type basis sets (BS's) [36]. The hybrid exchange-correlation functional WC1PBE composing of a PBE correlation part and a Wu-Cohen exchange part with a fractional mixing (16%) of the nonlocal Hartree-Fock exchange was used in this work [37]. All the self-consistent field (SCF) calculations were accomplished in the closed-shell form with a $8 \times 8 \times 8$ k-point mesh in the Brillouin zone based on the Monkhorst-Pack scheme [38] and a predefined "extra extra large" pruned DFT integration grid. The truncation criteria of the two-electrons integrals (Coulomb and HF exchange series) was set as 8, 8, 8, 8, and 16, and the energy convergence threshold with 10^{-9} Hartree for the SCF iterations was chosen for the sake of high accuracy. The convergence thresholds of the root-mean-square of the gradient and nuclear displacement for the geometry optimization were set to 0.00006 Hartree/bohr and 0.00012 bohr, respectively. The SCF convergence speed was facilitated by mixing 50% of the Hamiltonian matrix of the last cycle into the present one.

The local Gaussian-type BS's were chose as follows: for the atoms lighter than the beginning of the 3d transition metal series, the all-electron BS's 6-211d1G [39], 8-511d1G [40], 86-511d21G [41], 8-511d1G[42], 8-411d1G [43], 86-311d1G [44] were applied for Be, Mg, Ca, Al, O, S atoms, correspondingly. For other heavier atoms Sr, Ba, Ga, In, the small-core fully-relativistic effective core pseudo-potentials of the Stuttgart/Cologne group and their related valence BS's were adopted, and the diffuse functions with exponents less than 0.1 $bohr^{-2}$ in those valence BS's were removed in order to avoid numerical catastrophes [45,46].

Results and discussion

Structural properties

The crystal structure of spinel compounds is described by the ternary face-centered cubic lattice, with the space group Fd3m. Fig. 1 shows one unit cell of $MgAl_2O_4$ as an example of this structure. The A^{2+} cations occupy the tetrahedral (0, 0, 0) position, whereas the B^{3+} cations occupy the octahedral (0.625, 0.625, 0.625) position, where all coordinates are given in terms of the cubic lattice constant a. The X^{2-} anions are located at the (u, u, u) position; the value of the internal parameter u varies from host to host depending on the chemical composition [47].

In $MgAl_2O_4$ the Mg^{2+} ions occupy only 12.5% (or 1/8) of the available tetrahedral sites, and the Al^{3+} ions take a half of the available octahedral positions [49]. Thus, a large number of empty octahedral and tetrahedral cavities offer additional possibilities for the ion diffusion, defect formation, doping and co-doping with different chemical elements. In the normal spinel, all the A^{2+} and B^{2+} ions reside at the 8a and 16d sites, respectively. It is noted that all spinels whose properties were calculated in the present work were treated as the normal spinel.

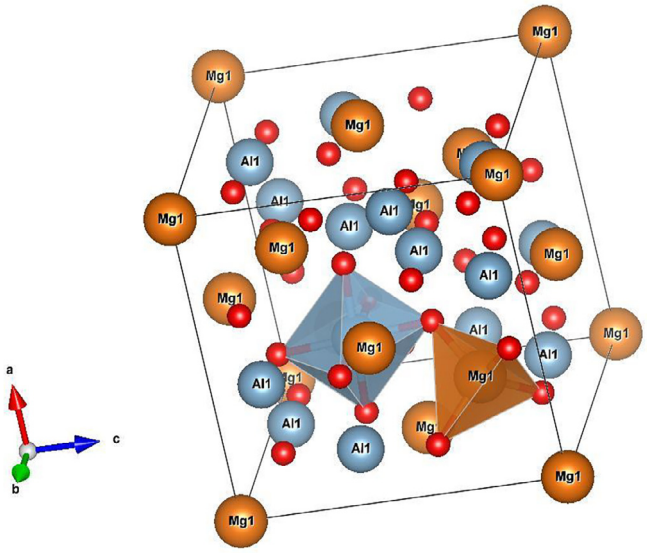

Fig. 1. One unit cell of $MgAl_2O_4$ as an example of the AB_2X_4 spinel structure. Oxygen ions are shown by small red spheres, Mg and Al ions are labeled. Coordination polyhedra around the A^{2+} and B^{3+} cations are shown. See text for more details. Drawn with VESTA [48]. (For interpretation of the references to color in this figure legend, the reader is referred to the web version of this article.)

Table 1
Empirical and theoretical lattice constants a (Å) and non-dimensional internal anion parameters u for various AB_2X_4 (A = Be, Mg, Ca, Sr, Ba; B = Al, Ga, In; X = O, S) spinels. The empirical lattice constants were obtained with the use of equations from Ref. [35]; the experimental lattice constants (if available) are given in the parenthesis.

Spinel	Empirical a_{emp}	Theoretical		Difference, $a_{emp} - a_{theor}$, %
		a_{theor}	u	
$BeAl_2O_4$	7.7999	7.67774	0.25449	1.57
$MgAl_2O_4$	8.1903	8.07782 (8.0898[a])	0.26363 (0.2633[a])	1.37
$CaAl_2O_4$	8.6102	8.43542	0.27034	2.03
$SrAl_2O_4$	8.8451	8.63962	0.27373	2.32
$BaAl_2O_4$	9.0568	8.87412	0.27734	2.02
$BeGa_2O_4$	8.0042	7.91310	0.25120	1.14
$MgGa_2O_4$	8.3947	8.31266 (8.2781[b])	0.26138 (0.2560[b])	0.98
$CaGa_2O_4$	8.8146	8.65987	0.26856	1.76
$SrGa_2O_4$	9.0494	8.85737	0.27216	2.12
$BaGa_2O_4$	9.2612	9.08114	0.27594	1.94
$BeIn_2O_4$	8.4895	8.50583	0.24514	−0.19
$MgIn_2O_4$	8.8800	8.91095 (8.8100[c])	0.25627 (0.3720[c])	−0.35
$CaIn_2O_4$	9.2999	9.24078	0.26399	0.64
$SrIn_2O_4$	9.5347	9.42531	0.26792	1.15
$BaIn_2O_4$	9.7465	9.63308	0.27208	1.16
$BeAl_2S_4$	9.3939	9.65739	0.25361	−2.80
$MgAl_2S_4$	9.7843	10.10359	0.26205	−3.26
$CaAl_2S_4$	10.2042	10.46870	0.26778	−2.59
$SrAl_2S_4$	10.4391	10.66922	0.27076	−2.20
$BaAl_2S_4$	10.6508	10.90140	0.27405	−2.35
$BeGa_2S_4$	9.5982	9.80705	0.25237	−2.18
$MgGa_2S_4$	9.9886	10.25493	0.26099	−2.67
$CaGa_2S_4$	10.4086	10.63103	0.26674	−2.14
$SrGa_2S_4$	10.6434	10.84726	0.26986	−1.92
$BaGa_2S_4$	10.8552	11.09535	0.27325	−2.21
$BeIn_2S_4$	10.0835	10.29296	0.24799	−2.08
$MgIn_2S_4$	10.4739	10.73795 (10.7109[d])	0.25718 (0.3832[d])	−2.52
$CaIn_2S_4$	10.8939	11.09873	0.26337	−1.88
$SrIn_2S_4$	11.1287	11.30724	0.26676	−1.60
$BaIn_2S_4$	11.3405	11.54230	0.27035	−1.78

[a] Ref. [52].
[b] Ref. [53].
[c] Ref. [54].
[d] Ref. [55].

The first step of the first-principles calculations for the solids is the geometry optimization, whose main purpose is to get the lowest total energy of a unit cell and smallest forces acting upon all atoms by allowing the atoms to move slightly around their equilibrium positions. Comparison of the obtained in this way theoretical lattice constants with the experimental ones (whenever available) can serve as an initial trustable criterion of reliability of the performed calculations. As a rule, the difference between the calculated and experimental lattice constants should not exceed a few percent at most.

The calculated (with the above-given calculations settings) lattice constants for all 30 studied spinels are listed in Table 1. For four spinels from the considered group the experimental structural data can be found. For the remaining 26 spinels, which are reported here for the first time, the initial lattice constant was estimated with the help of linear Eq. (1) from Ref. [35], standard Shannon ionic radii [50] and Pauling electronegativities [51] (see the Supporting Information (SI) file for further details), and the initial value of the internal parameter u was taken from the experimental measurement results of $MgAl_2O_4$ [52]. The obtained in this way values were used as an input for the calculations. The data from Table 1 suggest good agreement between the optimized and experimental/empirical lattice constants; the maximum relative error is −3.26%.

The overall trends in the behavior of the lattice constants with variation of both cations and anions are visualized in Figs. 2 and 3. In both figures the calculated values are shown by the symbols. If the first cation is kept, then the lattice constants increase in the Al → Ga → In direction. If the second cation is not changed, the lattice constants grow in the Be → Mg → Ca → Sr → Ba direction. If both cations are the same, but the anion is changed from oxygen to sulfur, the lattice constants increase as well. All these observations are in accordance with increased ionic radii of the considered chemical elements. The calculated data points were fitted to the linear functions (solid lines in both figures); the values of the correlation coefficient R^2 are close to unity in all cases.

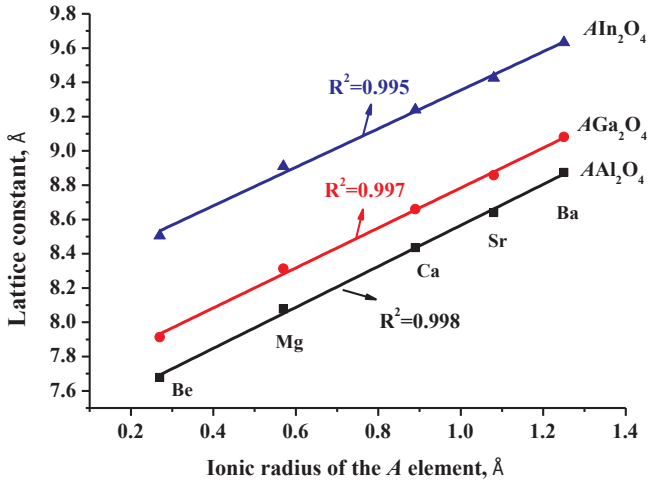

Fig. 2. Linear relations between the calculated lattice constants of spinel oxides and cations' ionic radii.

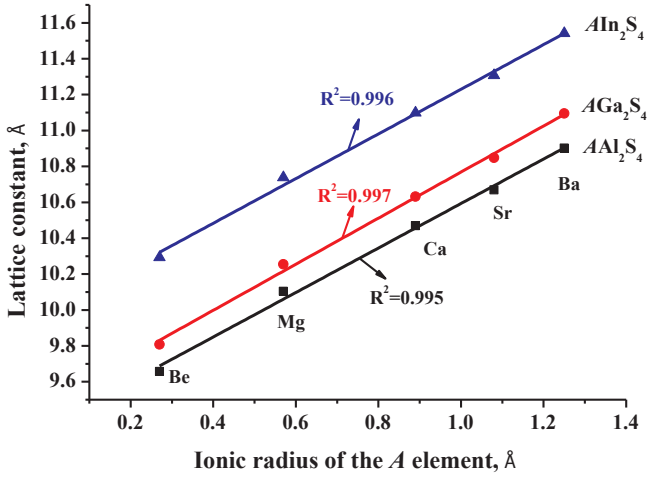

Fig. 3. Linear relation between the calculated lattice constants of spinel sulfides and cations' ionic radii.

The linear fitting equation for the calculated lattice constants using the ionic radii and electronegativities as the variables could be written as:

$$a = 1.33703(R_A + R_X) + 2.84713(R_B + R_X) + 0.15460(\chi_X - \chi_B) - 0.17489(\chi_X - \chi_A) + 0.10675 \quad (1)$$

where Pauling electronegativity scale and Shannon's ionic radii were used. This equation is consistent with Eq. (1) from Ref. [35], which could provide a convenient way to estimate the new spinel lattice constants.

Table 2
Calculated band gaps E_g (eV) for various spinel compounds AB_2X_4 (A = Be, Mg, Ca, Sr, Ba; B = Al, Ga, In; X = O, S) with space group Fd3m. (if available, the experimental data are given in bold).

Spinel	Band gaps		Transition types
	Γ-Γ	Γ-other k points	
$BeAl_2O_4$	8.439		Direct
$MgAl_2O_4$	7.160 (**7.8** [a])	7.147(SM)	Indirect
$CaAl_2O_4$	6.475	6.122(X)	Indirect
$SrAl_2O_4$	5.839	5.352(X)	Indirect
$BaAl_2O_4$	4.762	4.190(X)	Indirect
$BeGa_2O_4$	5.806	5.804(SM)	Indirect
$MgGa_2O_4$	5.132		Direct
$CaGa_2O_4$	4.746	4.637(X)	Indirect
$SrGa_2O_4$	4.288	3.904(X)	Indirect
$BaGa_2O_4$	3.407	2.807(X)	Indirect
$BeIn_2O_4$	3.352		Direct
$MgIn_2O_4$	3.529 (**3.4**[b])		Direct
$CaIn_2O_4$	3.843		Direct
$SrIn_2O_4$	3.630	3.604(L)	Indirect
$BaIn_2O_4$	3.040	2.864(X)	Indirect
$BeAl_2S_4$	3.554	3.508(SM)	Indirect
$MgAl_2S_4$	4.420	4.385(SM)	Indirect
$CaAl_2S_4$	4.457	4.278(X)	Indirect
$SrAl_2S_4$	3.913	3.581(X)	Indirect
$BaAl_2S_4$	3.289	2.812(X)	Indirect
$BeGa_2S_4$	2.160	2.013(SM)	Indirect
$MgGa_2S_4$	2.727	2.705(SM)	Indirect
$CaGa_2S_4$	2.610		Direct
$SrGa_2S_4$	2.152	1.982(X)	Indirect
$BaGa_2S_4$	1.659	1.262(X)	Indirect
$BeIn_2S_4$	2.350	2.313(SM)	Indirect
$MgIn_2S_4$	2.962 (**2.1**[c])		Direct
$CaIn_2S_4$	2.795		Direct
$SrIn_2S_4$	2.494		Direct
$BaIn_2S_4$	2.167	2.027(X)	Indirect

[a] Ref. [56].
[b] Ref. [57].
[c] Ref. [58].

Electronic properties

The electronic structure of a solid is a key factor that determines possible areas of its applications. Analysis of the calculated band structures for all studied spinels reveals that nearly all of them are the wide-band gap insulators, except for the sulfide spinels, which can be described as the semiconducting materials. The band gaps that are wider than 3–4 eV can accommodate many defects and impurity ions energy levels, which indicates high potential of many from the studied spinels for doping with various impurity ions for optical applications.

The majority of the calculated band structures are characterized by the indirect band gaps (Table 2). Comparison of the calculated and available experimental band gaps for three spinel compounds $MgAl_2O_4$, $MgIn_2O_4$, and $MgIn_2S_4$ shows good agreement (it is worthwhile to remind here that the conventional DFT-based methods usually underestimate the band gaps, whereas the hybrid DFT methods give the results much closer to the experimental values).

The origin of the calculated electronic bands can be understood using the density of states (DOS) diagrams. For the sake of brevity, all calculated band structure and DOS diagrams are shown in the SI file. In all spinels the top of the valence band is very flat; it is composed mainly of the oxygen 2p or sulfur 3p states. On the contrary, the dispersion of the electronic states at the conduction band bottom is well-pronounced, especially in the vicinity of the Brillouin zone center. The conduction bands in all spinels are made by the unoccupied s-, p, and d-states of both A and B cations. It can be noted that in eight spinels – $MgGa_2S_4$, $MgIn_2S_4$, $CaGa_2S_4$, $CaIn_2S_4$, $SrGa_2S_4$, $SrIn_2S_4$, $BaGa_2S_4$, $BaIn_2S_4$ the conduction band consists of two sub-bands separated by about 1 eV. The lowest part of the conduction band is composed of the Ga 4 s or In 5 s states, and the Ga 4p (or In 5p) with the s, p states of the first cation make the upper part of the conduction band.

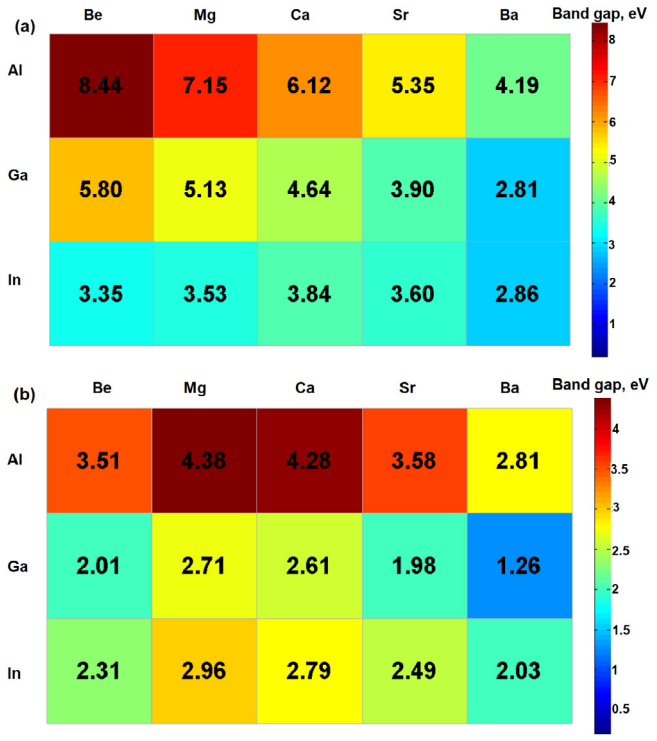

Fig. 4. Relations between the calculated band gaps (eV) and composition for the AB_2O_4 (a) and AB_2S_4 (b) (A = Be, Mg, Ca, Sr, Ba; B = Al, Ga, In) spinels.

The compositional-dependent variation of the band gaps is shown in Fig. 4. It is easy to see – by comparing the numbers in the corresponding squares – that the calculated band gaps for the oxide spinels are always wider than for their sulfide counterparts. Fig. 5 shows the overall trends in the variations of the calculated band gaps at the Brillouin zone center versus calculated lattice constants. For the XAl_2O_4 and XGa_2O_4 spinels the calculated band gaps decrease practically linearly with increasing lattice constants. For other four groups – XIn_2O_4, XAl_2S_4, XGa_2S_4, XIn_2S_4 – the Γ – Γ band gap slightly increases first, and then decreases.

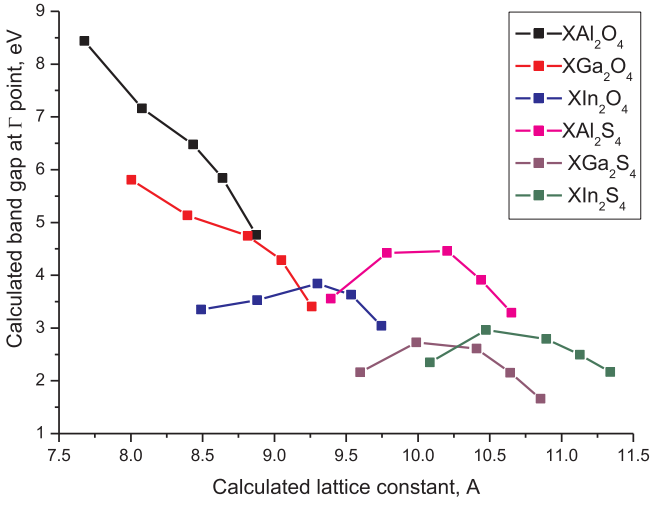

Fig. 5. Variation of the calculated Γ – Γ band gap versus calculated lattice costant in the considered groups of spinels.

Elastic properties

The elastic constants are important parameters to evaluate the stiffness and mechanical stability of solids. In general, the elastic constants C_{ij} form a symmetric 6 × 6 matrix, and knowledge of its components allows for calculating elastic response of a solid to any external stress. For the cubic crystal crystals, the non-zero components of that matrix are $C_{11} = C_{22} = C_{33}$, $C_{44} = C_{55} = C_{66}$, $C_{12} = C_{13} = C_{23}$, which gives three independent elastic constants only [59]. All calculated elastic parameters for the considered 30 spinel compounds are listed in Table 3 in the SI. The obtained values can be used to assess the mechanical stability of the considered materials, whose criteria for a cubic crystal are [59]:

$$C_{11} > 0,\ \ C_{44} > 0,\ \ C_{11} > |C_{12}|,\ \ (C_{11} + 2C_{12}) > 0 \tag{2}$$

As can be seen from Table 2, these conditions are satisfied for all considered AB_2X_4 compounds except for $BaAl_2S_4$, $SrGa_2S_4$, $BaGa_2S_4$ and $BaIn_2S_4$, because for these spinels the C_{11} value is smaller than C_{12} constant. Thus, the $BaAl_2S_4$, $SrGa_2S_4$, $BaGa_2S_4$ and $BaIn_2S_4$ crystals are not mechanically stable. Using the calculated C_{ij} values, several other important parameters of solids such as the shear modulus G, bulk modulus B and Debye temperature θ_D can be obtained from the following equations (valid for the cubic crystals only) [60–62]:

$$B_V = \frac{C_{11} + 2C_{12}}{3} \tag{3}$$

$$G_V = \frac{C_{11} - C_{12} + 3C_{44}}{5} \tag{4}$$

$$\frac{1}{B_R} = 3S_{11} + 6S_{12} \tag{5}$$

$$\frac{5}{G_R} = 4S_{11} - 4S_{12} + 3S_{44} \tag{6}$$

$$B = \frac{B_R + B_V}{2} \tag{7}$$

$$G = \frac{G_R + G_V}{2} \tag{8}$$

$$\theta_D = \frac{h}{k}\left(\frac{3n}{4\pi}\frac{N_A\rho}{M}\right)^{1/3} v_m \tag{9}$$

$$v_m = \left[\frac{1}{3}\left(\frac{2}{v_t^3} + \frac{1}{v_l^3}\right)\right]^{-1/3} \tag{10}$$

$$v_l = \sqrt{\frac{3B + 4G}{3\rho}},\ v_t = \sqrt{\frac{G}{\rho}} \tag{11}$$

where $h = 6.626 \times 10^{-34}$ J·s is the Planck's constant, $k_B = 1.381 \times 10^{-23}$ J/K is the Boltzmann constant, $N_A = 6.022 \times 10^{23}$ mol^{-1} is the Avogadro's number, ρ is the density, n is the number of atoms per one formula unit (7 in our case), and M is the molecular weight. The average, transverse and longitudinal sound velocities are denoted by v_m, v_t, v_l, correspondingly. Fig. 6 shows the composition-dependent bulk modulus values for all considered compounds. Two-dimensional representations of the calculated bulk moduli with added color showing the calculated values indicate a decreasing trend of the B values from the left upper to the right lower corners of the shown diagrams. The bulk moduli and Debye temperatures gradually decrease with increasing the atomic number from Be to Ba and from Al, Ga, In, which indicates that the crystal lattice gradually softens, and the highest frequencies of the lattice modes decrease due to the increased atomic weights, increased interatomic distances and, as a combined result of the two latter factors, decreased force constants of the normal modes. After the upper (Voigt, G_V) and lower (Reuss, G_R) shear moduli are estimated, it becomes possible to find the value of the anisotropy

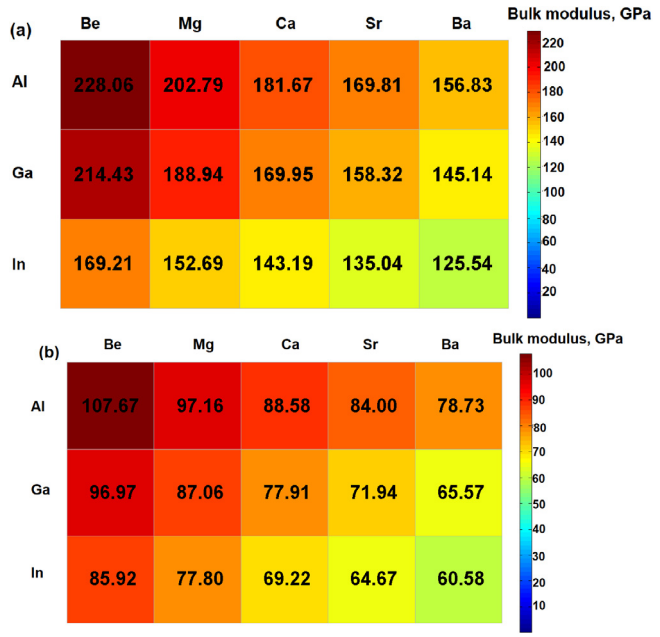

Fig. 6. Relations between the calculated bulk moduli (GPa) and composition for the AB_2O_4 (a) and AB_2S_4 (b) (A = Be, Mg, Ca, Sr, Ba; B = Al, Ga, In) spinels.

factor A_G [63]:

$$A_G = \frac{G_V - G_R}{G_V + G_R} \tag{12}$$

The higher is the A_G value, the more pronounced is the anisotropy of elastic properties for a given compound.

The bulk moduli variation indicates that the oxide spinels are considerably harder than the sulfide spinels. The calculated bulk moduli were fitted to the following equation with ionic radii and electronegativities as the variables:

$$B = -47.74886(R_A + R_X) - 108.59673(R_B + R_X) + 15.09573(\chi_X - \chi_B) + 4.14380(\chi_X - \chi_A) + 459.43240 \tag{13}$$

Physical reasons behind using the chosen variables in Eq. (13) are as follows: the interionic distances determine the force constants and compressibility of the chemical bonds. That is why the sums of the ionic radii of the neighboring ions enter the fit equations. However, the ions of the crystal lattice are not rigid spheres, and they are deformed because of the chemical bond formation. This is the reason why the differences of the electronegativities of the neighboring ions (which determine the degree of the bonds ionicity/covalency) are also considered as the fitting arguments. The overall quality of fit is visualized by Fig. 7 and the root-mean square deviation values of the fitted data of 9 GPa.

Also, the B/G ratio is an important parameter to distinguish between the brittle and ductile materials. If $B/G > 1.75$, the materials are ductile and if the ratio is opposite, the materials are brittle [64]. Application of this criterion shows that all studied spinels are ductile, except for these compounds (the B/G value is given in the parenthesis): $BeAl_2O_4$ (1.37), $BeGa_2O_4$ (1.63), $BeAl_2S_4$ (1.60), $BaGa_2S_4$ (-5.78), which turn out to be brittle (the last listed in this group spinel is mechanically unstable).

Although the considered spinels are all cubic, they still have a certain elastic anisotropy: response of the crystal lattice to the deformations applied along the (1 0 0), (1 1 0) and (1 1 1) directions will be different, because of different interatomic distances along those directions. Such anisotropy can be visualized by plotting directional dependence of the Young modulus E, which in the case of a cubic crystal is described by the following equation [65]:

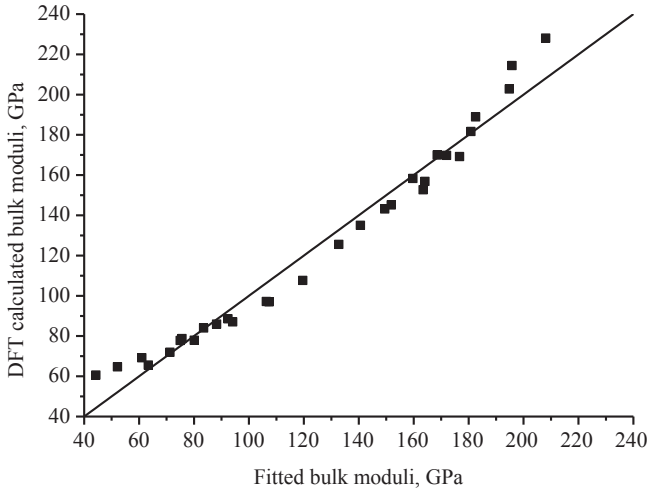

Fig. 7. Comparison between the calculated (vertical axis) and fitted by Eq. (13) (horizontal axis) bulk moduli for the studied 30 spinels. The straight line corresponds to one-to-one matching between both sets of data.

$$E(\vec{n}) = \frac{1}{S_{11} - \beta_1(n_1^2 n_2^2 + n_1^2 n_3^2 + n_2^2 n_3^2)} \quad (14)$$

where $\beta_1 = 2S_{11} - 2S_{12} - S_{44}$, S_{ij} are the matrix elements of the elastic compliance matrix given in Table 3 in the SI file and n_1, n_2, n_3 are the cosines of the angles between a given direction in the crystal lattice and the *a*, *b*, *c* crystallographic axes. For the elastically isotropic solid such a surface would be a sphere; however, in all considered cases its shape deviates from the spherical one, which is clearly illustrated by the figures in the SI file. The maximum E_{max} and minimum E_{min} values of the Young moduli can be determined from the following equations [65]:

$$E_{max} = \frac{3}{S_{11} + 2S_{12} + S_{44}}; E_{max} = \frac{1}{S_{11}}; \text{ if } \beta_1 > 0 \quad (15)$$

If $\beta_1 < 0$, then the "max" and "min" subscripts in these equations should be interchanged. Application of Eqs. (13) and (14) and analysis of the three-dimensional Young moduli in the SI file show that the maximal Young moduli values for these spinels are realized along the (1 1 1) direction, whereas the smallest ones are achieved along the (1 0 0), (0 1 0), (0 0 1) directions. This applies to all studied in the present paper spinels, that are mechanically stable, except for the case of $BeIn_2O_4$, for which$\beta_1 < 0$ and the greatest and smallest Young moduli are interchanged. The mechanically unstable spinels $BaAl_2S_4$, $SrGa_2S_4$, $BaGa_2S_4$ and $BaIn_2S_4$ appear to have negative lowest Young moduli values, which emphasizes their instability and impossibility to draw the corresponding three-dimensional representations for these compounds.

The Be-based spinels from Table 3 (SI file) are the most elastically isotropic compounds, among all 30 considered spinels. It is especially true for the Be-based oxide spinels, for which the Young moduli surfaces are nearly spherical. This is also confirmed by very small A_G values for these compounds. The Sr-based sulfide spinels are the mostly elastically anisotropic, which can be deduced from the shape of their Young moduli surfaces and high A_G values.

Finally, Fig. 8 offers composition-induced variation of the calculated Debye temperatures for the studies spinels. There is a monotonic decrease of the Debye temperatures from left to right and from top to bottom in the considered groups of spinels in Fig. 8, which is consistent with increase of the lattice constants (chemical bond lengths), decrease of the bulk moduli and overall softening of the crystal lattices formed by heavy ions.

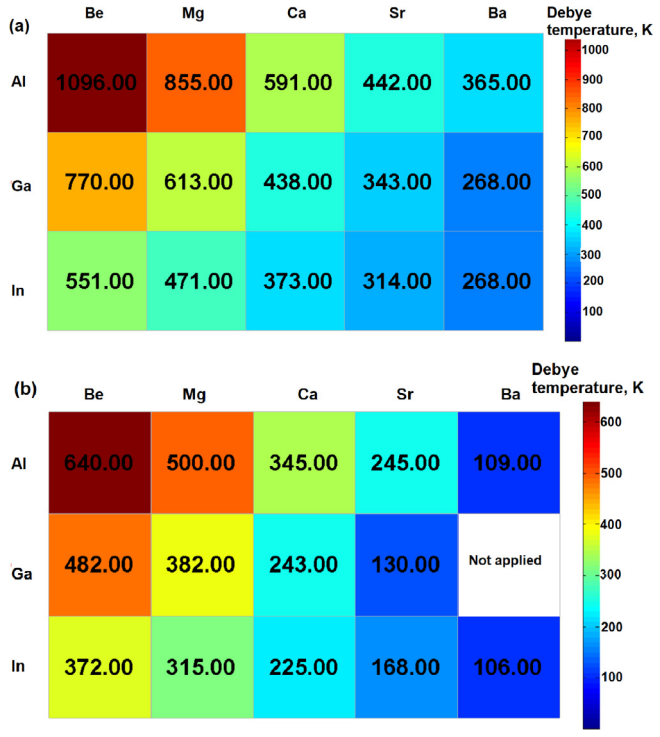

Fig. 8. Relations between the calculated Debye temperature (K) and composition for the AB_2O_4 (a) and AB_2S_4 (b) (A = Be, Mg, Ca, Sr, Ba; B = Al, Ga, In) spinels.

Conclusions

In this work, the results of calculations of the structural, electronic and elastic properties of 30 AB_2X_4 (A = Be, Mg, Ca, Sr, Ba; B = Al, Ga, In; X = O, S) spinel compounds are reported as an example of the high-throughput first-principles calculations aimed at uncovering systematic variation of different physical properties in the series of the isostructural crystals. In this way, the changes of the elastic and electronic properties of the studied compounds with the chemical composition were closely followed and represented graphically. The diagrams plotted in the paper reflect influence of the cation's and anion's changes on all calculated physical properties, including Debye temperatures. The calculated properties for 26 out of 30 studied spinels are given in the present paper for the first time, to the best of our knowledge. The calculated lattice constants and bulk moduli were fitted to the linear equations with the ionic radii and electronegativities as the variables. The presented results are an example of prediction of properties of unknown and/or non-synthesized yet compounds, which can be proved experimentally. The obtained systematic results could serve as a useful guide for search for new spinel compounds.

Acknowledgments

M.G. Brik thanks the supports from the National Recruitment Program of High-end Foreign Experts (Grant Nos. GDT20185200479 and GDW20145200225), the Programme for the Foreign Experts (Grant No. W2017011) and Wenfeng High-end Talents Project (Grant No. W2016-01) offered by Chongqing University of Posts and Telecommunications (CQUPT), Estonian Research Council grant PUT PRG111, and European Regional Development Fund (TK141). C.-G. Ma and Y. Tian acknowledge the supports of the Innovation and Entrepreneurship Program for Returned Overseas Chinese Scholars offered by Chinese Ministry and Chongqing Bureau of Human Resources and Social Security (Grant Nos. [2014] 167 and CX2018125), respectively, Scientific and Technological Research Program of Chongqing

Municipality Education Commission (Grant No. KJ1600415) and Doctoral Scientific Research Foundation of CQUPT (Grant Nos. A2008-59 and A2008-71). Y. Wang, D.-W. Yang and F.-Y. Liu appreciate the supports from the National Training Program of Innovation and Entrepreneurship for College Students offered by Chinese Ministry of Education (Grant No. 201410617001) and Research Training Program for Undergraduates of CQUPT (Grant No. A2018-39). W.-B. Chen thanks the supports of the National Natural Science Foundation of China (Grant No. 11804083) and Chongqing Natural Science Foundation (Grants No. cstc2017jcyjAX0418 and cstc2018jcyjAX0569).

Appendix A. Supplementary data

Supplementary data to this article can be found online at https://doi.org/10.1016/j.rinp.2019.102180.

References

[1] Priolo F, Gregorkiewicz T, Galli M, Krauss TF. Nat Nanotechnol 2014;9:19.
[2] Gmachl C, Capasso F, Sivco DL, Cho AY. Rep Progr Phys 2001;64:1533.
[3] Liu YM, Zhang X. Chem Soc Rev 2011;40:2494.
[4] Matussek M, Filapek M, Gancarz P, Krompiec S, Malecki JG, Kotowicz S, et al. Dyes Pigments 2018;159:590.
[5] Sadki H, Bourass M, Bennani MN, Bouachrine M. Res Chem Intermediat 2018;44:6071.
[6] Zhao ZF, Jing L, Wu ZH, Cheng J, Zhang MM, Hou YF. J Mater Sci 2018;53:15430.
[7] Veronica AM, Eveline VDW, Eduardo AP, Tomas T, Andres DLE. Chem Soc Rev 2018;47:7369.
[8] Zhang XF, Liu C, Zhang LZ, Wu JC, Xu BM. Dyes Pigments 2018;159:600.
[9] Kadyan S, Singh D. J Mater Sci – Mater El 2018;29:17277.
[10] Zawadzki M, Wrzyszcz J. Mater Res Bull 2000;35:109.
[11] Zamiri R, Salehizadeh SA, Ahangar HA, Shabani M, Rebelo A, Kumar JS, et al. Mater Chem Phys 2017;192:330.
[12] Nawale AB, Kanhe NS, Raut SA, Bhoraskar SV, Das AK, Mathe VL. Ceram Int 2017;43:6637.
[13] Nawle AC, Humbe AV, Babrekar MK, Deshmukh SS, Jadhav KM. J Alloys Compd 2017;695:1573.
[14] Vetter J, Novak P, Wagner MR, Veit C, Moller KC, Besenhard JO, et al. J Power Sour 2005;147:269.
[15] Hugh ST, O'Neill C, Navrotsky A. Am Mineral 1983;68:181.
[16] Ueda J, Back M, Brik MG, Zhuang YX, Grinberg M, Tanabe S. Opt Mater 2018;85:510.
[17] Brik MG, Papan J, Jovanović DJ, Dramićanin MD. J Lumin 2016;177:145.
[18] Luo W, Ma P, Xie TF, Dai JW, Pan YB, Kou HM, et al. Opt Mater 2017;69:152.
[19] Sakuma T, Minowa S, Katsumata T, Komuro S, Aizawa H. Opt Mater 2014;37:302.
[20] Brik MG, Nazarov M, Ahmad-Fauzi MN, Kulyuk L, Anghel S, Sushkevich K, et al. J Lumin 2012;132:2489.
[21] Brik MG, Nazarov M, Ahmad-Fauzi MN, Kulyuk L, Anghel S, Sushkevich K, et al. J Alloys Compd 2013;550:103.
[22] da Silva MAFM, Carvalho ICS, Cella N, Bordallo HN, Sosman LP. Opt Mater 2013;35:543.
[23] Kambale RC, Song KM, Koo YS, Hur N. J Appl Phys 2011;110. 053910.
[24] Omkaram I, Rao BV, Buddhudu S. J Alloys Compd 2009;474:565.
[25] Ladgaonkar BP, Kolekar CB, Vaingankar AS. B MaterSci 2002;25:351.
[26] Hong JF, Mato K, Roland S, Kornelius N, Eckhard P, Dietrich H, et al. Nat Mater 2006;5:627.
[27] Wu GP, Wang J, Ding W, Nie Y, Li L, Qi XQ, et al. Angew Chem Int Edit 2016;55:1340.
[28] Prasad SAV, Deepty M, Ramesh PN, Prasad G, Srinivasarao K, Srinivas C, et al. Ceram Int 2018;44:10517.
[29] Lushchik A, Dolgov S, Feldbach E, Pareja R, Popov AI, Shablonin E, et al. Nucl Instr Meth Phys Res 2018;435:31.
[30] Bouhemadu A, Khenata R, Zerarga F. Comput Mater Sci 2007;39:709.
[31] Bouhemadu A, Khenata R, Zerarga F. Eur Phys J B 2007;56:1.
[32] Semari F, Khenata R, Rabah M, Bouhemadou A, Bin Omran S, Reshak AH, et al. J Solid State Chem 2010;183:2818.
[33] Brik MG. J Phys Chem Solids 2010;71:1435.
[34] Abbas SA, Rashid M, Faridi MA, Saddique MB, Mahmood A, Ramay SM. J Phys Chem Solids 2018;113:157.
[35] Brik MG, Suchocki A, Kaminska A. Inorg Chem 2014;53:5088.
[36] Dovesi R, Saunders VR, Roetti C, Orlando R, Zicovich-Wilson CM, Pascale F, et al. CRYSTAL14 User's Manual. Torino: University of Torino; 2014.
[37] Demichelis R, Civalleri B, Ferrabone M, Dovesi R. Int J Quantum Chem 2009;110:406.
[38] Monkhorst HJ, Pack JD. Phys Rev B 1976;13:5188.
[39] Baima J, Erba A, Rerat M, Orlando R, Dovesi R. J Phys Chem C 2013;117:12864.
[40] Valenzano L, Noel Y, Orlando R, Zicovich-Wilson CM, Ferrero M, Dovesi R. Theor Chem Acc 2007;117:991.
[41] Valenzano L, Torres FJ, Doll K, Pascale F, Zicovich-Wilson CM, Dovesi R. Z Phys Chem 2006;220:893.
[42] Catti M, Valerio G, Dovesi R, Causa M. Phys Rev B 1994;49:14179.
[43] Bredow T, Jug K, Evarestov RA. Phys Status Solidi B 2006;243:R10.
[44] Lichanot A, Apra E, Dovesi R. Phys Status Solidi B 1993;177:157.
[45] Lim IS, Stoll H, Schwerdtfeger P. J Chem Phys 2006;124. 034107.
[46] Metz B, Stoll H, Dolg M. J Chem Phys 2000;113:2563.
[47] D'Arco P, Silvi B, Roetti C, Orlando R. J Geophys Res 1991;96:6107.
[48] Momma K, Izumi F. J Appl Crystallogr 2011;44:1272.
[49] Müller U. Inorganic structural chemistry. New York: Wiley & Sons; 1993.
[50] Shannon RD. Acta Crystallogr A 1976;32:751.
[51] Pauling L. J Am Chem Soc 1932;54:3570.
[52] Finger LW, Hazen RM, Hofmeister AM. Phys Chem Miner 1986;13:215.
[53] Garcia CP, Rasines I. Z Krist-Cryst Mater 1982;160:33.
[54] Barth TFW, Posnjak E. Z Krist-Cryst Mater 1932;82:325.
[55] Gastaldi L, Lapiccirella A. J Solid State Chem 1979;30:223.
[56] Bortz ML, French RH, Jones DJ, Kasowski RV, Ohuchi FS. Phys Scripta 1990;41:537.
[57] Ueda N, Omata T, Hikuma N, Ueda K, Mizoguchi H, Hashimoto T, et al. Appl Phys Lett 1992;61:1954.
[58] Sirimanne PM, Sonoyama N, Sakata T. J Solid State Chem 2000;154:476.
[59] Nye JF. Physical Properties of Crystals: their representation by tensors and matrices. New York: Oxford University Press; 1985.
[60] Anderson OL. J Phys Chem Solids 1963;24:909.
[61] Poirier JP. Introduction to the physics of the Earth's interior. Cambridge: Cambridge University Press; 2000.
[62] Schreiber E, Anderson OL, Soga N. Elastic constants and their measurements. New York: McGraw-Hill; 1973.
[63] Zhou W, Liu LJ, Li BL, Wu P, Song QG. Comp. Mater. Sci. 2009;46:921.
[64] Pugh SF. Lond. Edinb. Dubl. Phil. Mag. 1954;45:823.
[65] Cazzani A, Rovati M. Int. J. Solids Struct. 2003;40:1713.